Extracting the Buoyancy-Driven Atlantic Meridional Overturning Circulation

SARAH M. LARSON

Department of Marine, Earth, and Atmospheric Sciences, North Carolina State University, Raleigh, North Carolina

MARTHA W. BUCKLEY

Department of Atmospheric, Oceanic, and Earth Sciences, George Mason University, Fairfax, Virginia

AMY C. CLEMENT

Department of Atmospheric Sciences, Rosenstiel School of Marine and Atmospheric Sciences, University of Miami, Miami, Florida

(Manuscript received 1 August 2019, in final form 4 March 2020)

ABSTRACT

Variations in the Atlantic meridional overturning circulation (AMOC) driven by buoyancy forcing are typically characterized as having a low-frequency time scale, interhemispheric structure, cross-equatorial heat transport, and linkages to the strength of Northern Hemisphere gyre circulations and the Gulf Stream. This study first tests whether these attributes ascribed to the AMOC are reproduced in a coupled model that is mechanically decoupled and, hence, is only buoyancy coupled. Overall, the mechanically decoupled model reproduces these attributes, with the exception that in the subpolar gyre, buoyancy drives AMOC variations on interannual to multidecadal time scales, yet only the multidecadal variations penetrate into the subtropics. A stronger AMOC is associated with a strengthening of the Northern Hemisphere gyre circulations, Gulf Stream, and northward oceanic heat transport throughout the basin. We then determine whether the characteristics in the mechanically decoupled model can be recovered by low-pass filtering the AMOC in a fully coupled version of the same model, a common approach used to isolate the buoyancy-driven AMOC. A major conclusion is that low-pass filtering the AMOC in the fully coupled model reproduces the buoyancy-driven AMOC pattern and most of the associated attributes, but not the statistics of the temporal variability. The strength of the AMOC–Gulf Stream connection is also not reproduced. The analyses reveal caveats that must be considered when choosing indexes and filtering techniques to estimate the buoyancy-driven AMOC. Results also provide insight on the latitudinal dependence of time scales and drivers of ocean circulation variability in coupled models, with potential implications for measurement and detection of the buoyancy-driven AMOC in the real world.

1. Introduction

The Atlantic meridional overturning circulation (AMOC) comprises a northward flowing branch of warm upper ocean waters counterbalanced by a southward-flowing branch of cold deeper ocean waters that together assemble an overturning cell. The AMOC is characterized by cross-equatorial heat transport into the Northern Hemisphere (NH); thus the AMOC serves as an important factor in the global redistribution of heat within the climate system (Trenberth and Caron 2001; Kuhlbrodt et al. 2007; McCarthy et al. 2015; Buckley and Marshall 2016; Lozier 2012). AMOC-driven heat transport has been linked to key attributes of current-day climate, including the latitudinal position of the intertropical convergence zone (Kang et al. 2008, 2009; Frierson et al. 2013; Marshall et al. 2014) and the relatively warmer climate in the NH compared to the Southern Hemisphere (SH; Feulner et al. 2013; Marshall et al. 2014).

Low-frequency variability in the AMOC is associated with large-scale variations in meridional ocean heat transports (e.g., Dong and Sutton 2002; Delworth and Zeng 2012; Johns et al. 2011; Zhang and Zhang 2015). Through its role in ocean heat transport, variations in the AMOC strength have been linked to numerous climate impacts [see review by Zhang et al. (2019)], including sea ice variability (e.g., Yeager et al. 2015; Li et al. 2018), NH climate (e.g., Pohlmann et al. 2006), and

Corresponding author: Sarah M. Larson, slarson@ncsu.edu

DOI: 10.1175/JCLI-D-19-0590.1

low-frequency North Atlantic SST variability (e.g., Zhang et al. 2019). The AMOC has also been identified as a prospect for enhancing decadal climate prediction efforts (Dunstone and Smith 2010; Yeager and Robson 2017), as the predictability of climate on long time scales lies in the interaction of the atmosphere with slower components of the climate system, including the ocean. Low-frequency AMOC-driven variations thus potentially serve as a source of predictability of climate on longer time scales. For these reasons measuring, predicting, and understanding changes in AMOC strength are key foci in both the climate and oceanographic communities.

Modeling studies have identified a link between changes in the AMOC strength and variations in the NH gyre circulations, as well as shifts in the Gulf Stream path (de Coëtlogon et al. 2006; Joyce and Zhang 2010). Topographic coupling of the overturning and gyre circulations is expected, as bottom pressure torques have been shown to play a dominant role in the vorticity budget of both the barotropic gyre circulation and the AMOC (Yeager 2015). Despite this, modeling studies do not agree on the sign of the relationship between variations in the AMOC and gyre circulations. In some studies, a strengthening of the AMOC is associated with a strengthening of the subtropical and subpolar gyre circulations and a strengthening and northward shift of the Gulf Stream (GS) path (Böning et al. 2006; de Coëtlogon et al. 2006; Yeager 2015). These studies suggest that the relationship between changes in the AMOC, the gyre circulations, and GS may be due to the fact that they are driven by common forcing (e.g., the North Atlantic Oscillation) or because the GS transport is, by definition, included in the meridional overturning streamfunction often used to define the AMOC. In another group of studies, a strengthening of the AMOC is associated with a weakening of the subpolar gyre and southward shifts in the GS path (Zhang 2008; Zhang et al. 2019). In these studies, buoyancy forcing and deep ocean variations are cited as the driving process, with increases in the strength of the Deep Western Boundary Current leading to an increase in the strength of the Northern Recirculation Gyre and a southward shift in the GS path (Zhang and Vallis 2007; Joyce and Zhang 2010; Zhang et al. 2019).

Untangling the relative contribution of buoyancy versus wind variability in driving intrinsic AMOC variations is of particular interest in predicting the associated impacts and characteristics, as wind and buoyancy are thought to drive overturning variability on different time scales (e.g., Buckley and Marshall 2016). Interannual AMOC variations, hereafter referred to as high-frequency variability, have been linked to wind variability (Biastoch et al. 2008; Xu et al. 2014; Roberts et al. 2017) and hence likely have limited predictability (Sinha et al. 2013). Decadal and longer AMOC variations, hereafter referred to as low-frequency variability, are thought to be predominantly driven by buoyancy variations (Biastoch et al. 2008; Medhaug et al. 2012; Polo et al. 2014; Yeager and Danabasoglu 2014) and have higher predictability (Keenlyside et al. 2008; Dunstone and Smith 2010; Msadek et al. 2010). Typically, variations in deep convection and water mass formation have been thought to drive the AMOC at low frequencies, but recent work has called this into question, as there is no direct observational link between water mass formation and the AMOC (Lozier 2010, 2012).

The characteristics typically ascribed to buoyancy-driven AMOC variations include 1) low-frequency, meridionally coherent AMOC variations with a maximum in the NH subpolar gyre, associated with 2) large-scale ocean heat transport variations, and 3) connection to variations in the strength of the NH gyre circulations. We will henceforth refer to AMOC variations with these attributes as the canonical or interhemispheric AMOC.

However, it is unclear where and on what time scales these attributes should be detectable in the real ocean and in coupled models. For example, detection of low-frequency AMOC variability in the subtropics, where the RAPID array (Srokosz and Bryden 2015) is located, is difficult, as the variability is dominated by wind-driven AMOC variations on shorter time scales (Cunningham et al. 2007; Baehr et al. 2008; Biastoch et al. 2008; Zhao and Johns 2014). Böning et al. (2006) argue that in addition to wind variability masking the buoyancy-driven signal, convectively driven AMOC variations originating in the subpolar latitudes weaken as they are communicated southward, further impeding detectability in the subtropics. Observations of the AMOC in the subpolar gyre, now being collected as part of the Overturning in the Subpolar North Atlantic Program (OSNAP; Lozier et al. 2017), may provide a more favorable location for understanding buoyancy-forced AMOC changes, but it is unclear how long a time series one needs in order to observe meridionally coherent, buoyancy-driven AMOC changes.

In the literature, fully coupled model studies often low-pass filter the AMOC in an attempt to remove the high-frequency wind-driven variations and estimate the buoyancy driven component (e.g., Cheng et al. 2013; Yeager and Danabasoglu 2014). That said, it is unclear whether the resulting temporally smoothed overturning indeed recovers the same variability had anomalous wind-driven AMOC variability simply been absent.

Insight can be gained about isolating the buoyancy-driven AMOC from modeling experiments. Previously, ocean and ocean–sea ice models with prescribed surface

flux forcing datasets (hereafter, Ocn_{flux} experiments) have been used to separate the relative contributions of buoyancy versus wind forcing to AMOC variations. In such studies, the buoyancy-driven AMOC contribution is isolated by forcing the ocean (and sea ice model, if available) with climatological momentum fluxes and time-varying heat (and freshwater, if available) fluxes. The prescribed fluxes and atmospheric state variables either originate from observational reanalyses (Eden and Willebrand 2001; Biastoch et al. 2008; Polo et al. 2014; Robson et al. 2012; Yeager and Danabasoglu 2014) or coupled model runs (e.g., Delworth and Greatbatch 2000; Buckley et al. 2012). Overall, these studies find that buoyancy forcing is the primary contributor to low-frequency, interhemispheric AMOC variability, whereas wind variability generates high-frequency variations and interhemispheric asymmetry, yet also contributes to decadal variations (Böning et al. 2006; Biastoch et al. 2008). The AMOC response to wind and buoyancy is also argued to be approximately linear (Biastoch et al. 2008; Polo et al. 2014; Yeager and Danabasoglu 2014).

In this work, we separate out the anomalous wind-driven contribution to AMOC variations from the buoyancy-driven contribution in a *coupled model* framework. This so-called mechanically decoupled (MD) approach (Larson et al. 2018) results in purely buoyancy-driven climate variations; hence the AMOC in the MD is purely buoyancy forced. This experimental framework is first invoked to test whether the typical attributes ascribed to the buoyancy-driven AMOC indeed emerge in a coupled model climate that lacks anomalous wind-driven ocean variability. The obvious advantage of the MD approach to the Ocn_{flux} experiments is that a coupled framework allows the exploration of coupled air–sea modes and the atmospheric response to the ocean state. The second goal is to determine whether the characteristics that describe the buoyancy-driven AMOC in the MD emerge from a fully coupled (FC) version of the same model when low-pass filtering the AMOC, a strategy often employed in FC model studies. Differences between the MD AMOC and low-frequency FC AMOC then reveal caveats that must be considered when using a filtering approach to estimate the buoyancy-driven AMOC in FC models.

2. Coupled model approach

a. Fully coupled CCSM4

This study utilizes the National Center for Atmospheric Research (NCAR) Community Climate System Model version 4 (CCSM4; Gent et al. 2011) with nominal 1° horizontal resolution and preindustrial forcing. The fully coupled (FC) model consists of atmosphere, land, ocean, and sea ice models that exchange fluxes and fields through a flux coupler. The ocean model is the Parallel Ocean Program version 2 (POP2; Smith et al. 2010), consisting of 60 vertical levels with a vertical spacing of 10 m in the upper 160 m and coarser vertical resolution at depth. The sea ice model is the Community Ice Code version 4 (Hunke and Lipscomb 2008). The atmosphere model is the Community Atmosphere Model version 4, consisting of 26 vertical levels and a finite-volume core (Neale et al. 2013). The land model is the Community Land Model version 4 (Oleson et al. 2008). The FC data used in this study are from a 1300-yr integration accessed from the NCAR Earth System Grid online repository and are identical to the simulation analyzed in Danabasoglu et al. (2012b). The ocean and sea ice models match those in the Yeager and Danabasoglu (2014) Ocn_{flux} study. Further description of ocean variability simulated in POP2 is found in Danabasoglu et al. (2012a). Similar to Danabasoglu et al. (2012b), only years 700–1300 are analyzed due to the slow deep ocean spinup occurring prior to year 700.

In the FC, the atmosphere and ocean communicate through thermal fluxes, freshwater fluxes, and momentum fluxes. Thermal fluxes consist of both turbulent air–sea heat exchanges, including sensible and latent heat fluxes; radiative heat fluxes, including shortwave and longwave solar radiation; and heat flux due to snow and ice melt. Freshwater fluxes include precipitation, evaporation, river runoff, and sea ice melt. Momentum fluxes represent wind stress coupling to the ocean.

b. Mechanically decoupled CCSM4

To analyze the buoyancy-driven ocean circulation in CCSM4, we utilize a mechanically decoupled (MD) version of the model (Larson et al. 2018). In the MD version, anomalous momentum coupling is disengaged by replacing the wind stress passed from the flux coupler to the ocean with the seasonal cycle of CCSM4/CESM wind stress. This means that anomalous wind stress does not dynamically force the ocean component of the model, and the ocean component only experiences the wind stress annual cycle. All other advantages of the FC configuration remain intact in the MD, including unconstrained buoyancy fluxes and atmospheric dynamics. The mean ocean circulation and anomalous ocean dynamics that are unrelated to anomalous wind stress are fully represented. The MD approach's treatment of air–sea fluxes allows for consistent fluxes between the atmosphere and ocean, and, as a result, coupled atmosphere–ocean modes are possible.

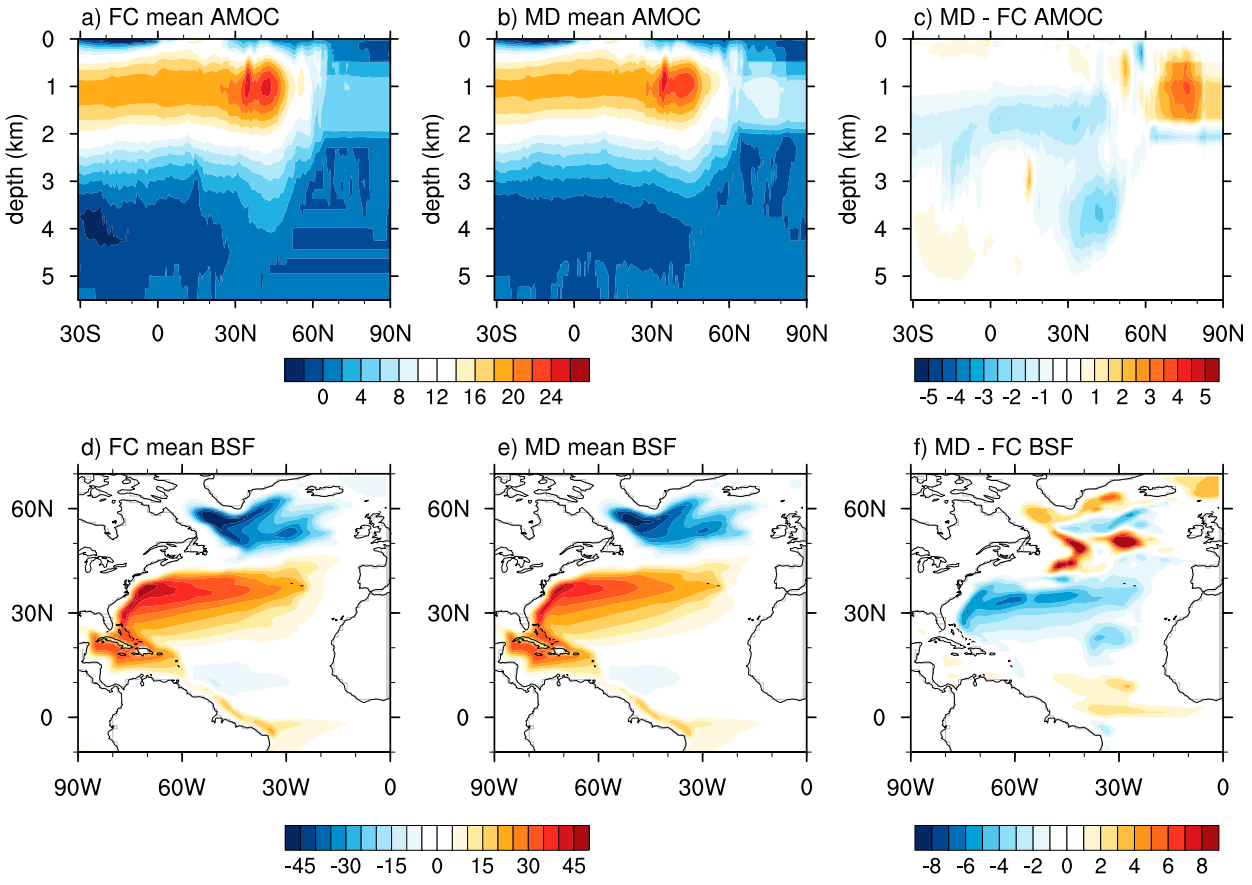

FIG. 1. Annual mean AMOC in CCSM4 in the (a) FC and (b) MD, and (c) their difference. (d)–(f) As in (a)–(c), but for annual mean barotropic streamfunction (BSF). Units are Sverdrups (Sv).

The MD is a preindustrial configuration and includes identical model components and resolution as the FC. The MD is branched from a FC version of the model. Both the FC and MD are buoyancy coupled but only the FC includes momentum coupling. Similar to the FC, the MD is "free-running" and can be integrated forward in time indefinitely. Additional details for the implementation of the MD configuration within the model code are located in the appendix. Assume for the remainder of this study that "FC" refers to years 700–1300 of the FC simulation integrated at NCAR and "MD" refers to years 700–1300 of an MD simulation integrated at the University of Miami (i.e., the MD is not branched from the NCAR FC model).

c. *Verification of the MD simulation: Mean state*

The MD qualitatively reproduces the mean AMOC and gyre circulations seen in the FC model. The maximum mean strength of the AMOC is similar (25.7 Sv; 1 Sv $\equiv$ $10^6\,m^3\,s^{-1}$) in MD and 26.1 Sv in FC) and in both models the maximum occurs near 1 km in depth (Figs. 1a–c). However, there are some quantitative differences, which are mainly the result of the mean wind stress being slightly different in the MD than FC. (This is because the mean wind stress in MD comes from a 100-yr climatology of a FC simulation integrated at the University of Miami, not the full 700-yr NCAR simulation; see appendix for additional details). South of 60°N, the MD AMOC is slightly shallower and weaker than the AMOC in the FC. In the South Atlantic, the MD surface westerlies are 10%–15% weaker than in the FC, which may contribute to the overall weaker AMOC strength as expected from reduced Ekman-induced upwelling of colder deep waters. Poleward of 60°N there is a relatively shallow, local overturning cell, which may be related to an Ekman overturning cell driven by polar easterlies or a local overturning cell driven by overflow transports. This cell is stronger in the MD, perhaps due to enhanced polar easterlies or increased overflow transports. The MD mean barotropic streamfunction (BSF) is approximately 5 Sv weaker in the center of the subtropical gyre than in the FC. The mean northward oceanic heat transport (OHT) in the MD closely reproduces the FC climatology (Fig. 2).

3. Buoyancy-driven AMOC characteristics

a. *Low-frequency meridionally coherent AMOC variations*

In this section we compare AMOC variations in the MD and FC simulations. We show that the MD simulation produces low-frequency, meridionally coherent AMOC variations. We also demonstrate that low-pass filtering the FC model's AMOC does not lead to AMOC variations that match the temporal statistics of the MD, but a similar dominant pattern of variability is observed.

1) TOTAL AMOC VARIANCE

First, we consider the total AMOC variance in the FC and MD experiments. In the MD, the total buoyancy-driven AMOC anomaly variance is consistent with an overturning cell with maximum in the NH subpolar gyre (Fig. 3b). The maximum variance occurs near 45°N at depths between 1 and 3 km. The FC produces a similar maximum between 40° and 50°N (Fig. 3a) but overall, the FC AMOC has larger variance than the MD everywhere, especially in the subtropics (Fig. 3c). Specifically, wind variability contributes to at least 80% of the AMOC variability in the upper 1 km from 30°S to 30°N. In this region, wind variability is a key contributor to the overturning variability in observations (Cunningham et al. 2007; Zhao and Johns 2014), including that associated with shallow subtropical overturning cells (Zhang et al. 2003). At depths between 2 and 3 km in the low latitudes and poleward of 30°N, up to 80% of the FC AMOC variance can be reproduced by buoyancy coupling alone (Fig. 3c).

Following previous approaches, we low-frequency filter the FC AMOC (hereafter, FC_{LF}) in an attempt to extract the buoyancy-driven signal. This is done by applying a low-pass Lanczos filter with a 10-yr cutoff. Does low-pass filtering the FC AMOC result in the same AMOC variance pattern as in the MD? The wind-driven variance in the subtropics is significantly reduced in the FC_{LF} and a maximum representing the NH centroid remains (Fig. 3d). For a consistent comparison, we also apply the same filter to the MD data (hereafter, MD_{LF}; Fig. 3e). At low frequencies, the MD_{LF} has higher variance than the FC_{LF} by at least 50% at depths around 2–3 km where the AMOC extends through the subtropics and into the SH (Fig. 3f). Indeed, in forced hindcast experiments using CESM1 configured with the same ocean model as in our experiments, Yeager (2015) argues that high-latitude buoyancy forcing drives southward signal propagation into the subtropical gyre with maximal impact on the AMOC at 1–3-km depths. So, if this AMOC signal is buoyancy-driven and the FC includes such variability, why is the signal weaker in the FC model? There are two possibilities. Either wind forcing in the subtropical gyre is sufficiently large to swamp the buoyancy-forced signal or wind forcing disrupts the meridional communication of the buoyancy-forced signal. The latter is consistent with reduction of the buoyancy-driven signal as it penetrates southward out of the subpolar gyre (Böning et al. 2006). Overall, low-pass filtering the FC data produces a similar AMOC variance pattern as the buoyancy-driven AMOC in the MD, but the amplitude of the variance differs at depth, and specifically is lower by roughly 50%.

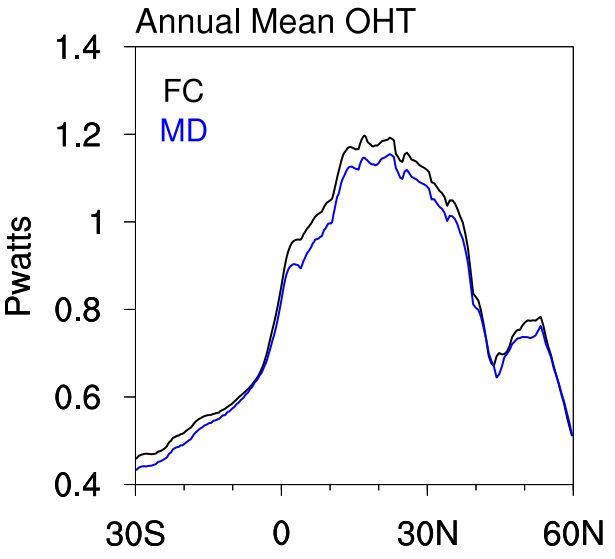

FIG. 2. Annual mean northward oceanic heat transport (OHT) due to Eulerian-mean advection over the Atlantic basin. Units are PW. Other contributions to the OHT are ignored, as they are at least one order of magnitude smaller than the contribution from Eulerian-mean advection (when using annual data).

Comparing the MD and MD_{LF} AMOC variance reveals on what time scales buoyancy drives the variations. In the subtropics, only a modest decrease in variance occurs after removing high frequencies (MD → MD_{LF}), demonstrating that the buoyancy-driven subtropical AMOC variability in the MD is primarily at low frequencies. On the other hand, high-frequency buoyancy forcing clearly enhances AMOC variance poleward of 40°N.

2) TEMPORAL VARIABILITY

Second, we consider the spectral characteristics of the variability in AMOC strength at each latitude in the FC and MD. Similar to Buckley and Marshall (2016), we calculate the annual AMOC strength as the maximum of the overturning streamfunction $\psi(y, z, t)$ at each latitude,

$$\psi_{max}(y,t) = \max_z \psi(y,z,t), \quad (1)$$

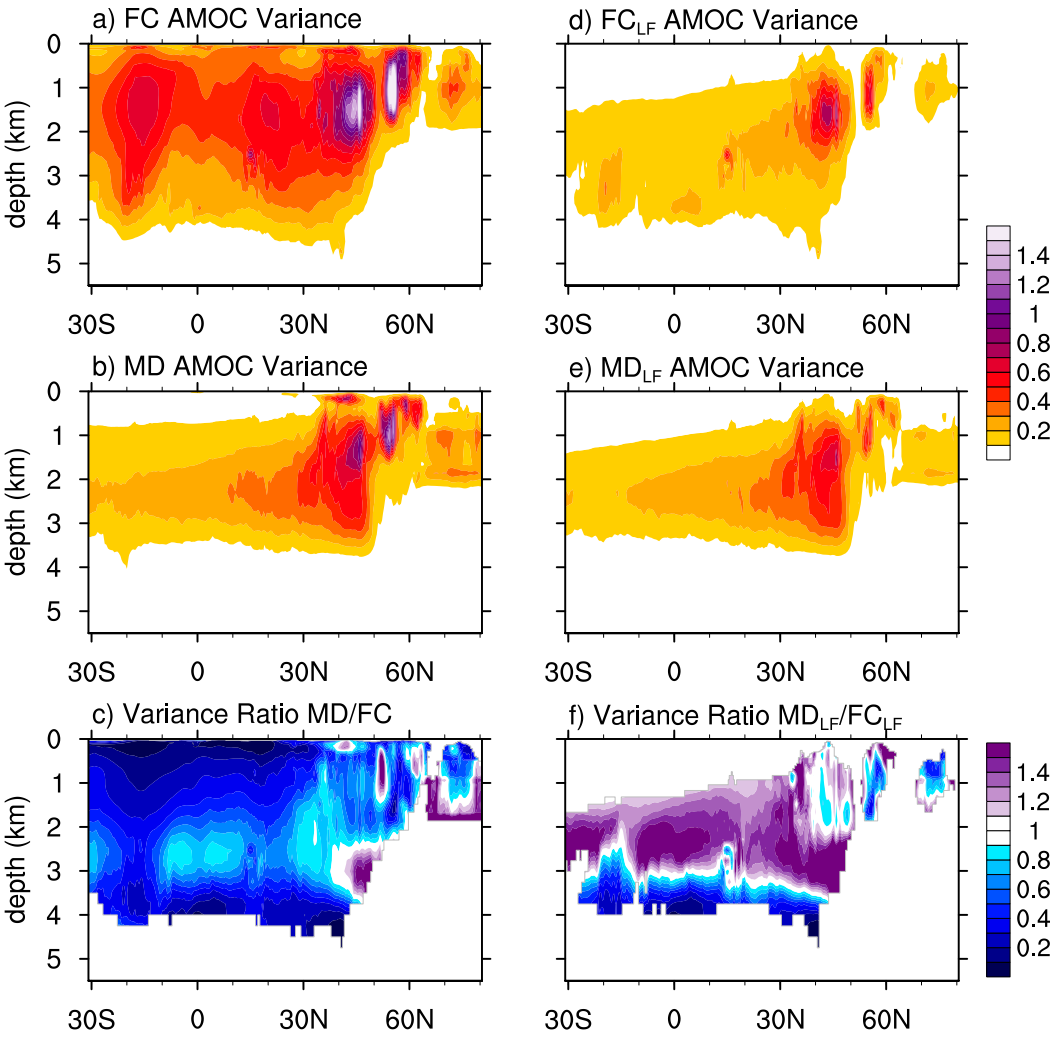

FIG. 3. Variance of annual AMOC anomalies for the (a) FC and (b) MD, and (c) their ratio. (d)–(f) As in (a)–(c), but for low-pass filtered annual AMOC anomalies. The filter is a low-pass Lanczos filter with a 10-yr cutoff. For (c) and (f), ratios are set to zero where the FC variance is <0.1 to avoid misleadingly large ratios based on the statistics of very small numbers, often near topography.

which occurs at depth $z_{\max}(y, t)$. The depth $z_{\max}$ is restricted to be below 300-m depth, and we have verified that the algorithm does not isolate subtropical overturning cells. This yields one AMOC strength time series per latitude. We next compute the spectrum of $\psi_{\max}(y, t)$ at each latitude from 30°S to 60°N and display the results as a time scale-by-latitude contour spectra (Figs. 4a,b) to provide a comprehensive picture of the time scales that contribute to the AMOC at each latitude. The standardized contour spectra (Figs. 4c,d) are similar to the contour spectra except that the time series of $\psi_{\max}(y, t)$ at each latitude is standardized (to have a standard deviation of one) prior to computation of the spectra. This method accentuates the dominant frequencies at each latitude, even if the total variance of $\psi_{\max}(y, t)$ at a given latitude is small.

We also plot the spectra of the maximum AMOC strength ($\text{AMOC}_{\max}$), an index that is often used by the community to measure the strength of the AMOC (Figs. 5a,b). $\text{AMOC}_{\max}$ is calculated as the maximum of $\psi_{\max}(y, t)$ over latitudes 20°–65°N. Since the maximum mean AMOC strength is located at ~45°N (see Figs. 1a,b), $\text{AMOC}_{\max}$ is expected to extract the time scales and amplitude of AMOC variability in that region. The spectra at 26°N (Figs. 5c,d) are also included to depict subtropical variability that is primarily wind-driven. To test the robustness of different peaks in the full 600-yr time series spectra (black thin lines), we break the data up into four nonoverlapping 150-yr periods, calculate the spectra, and plot the average of the four spectra (black bold lines). The window-averaged

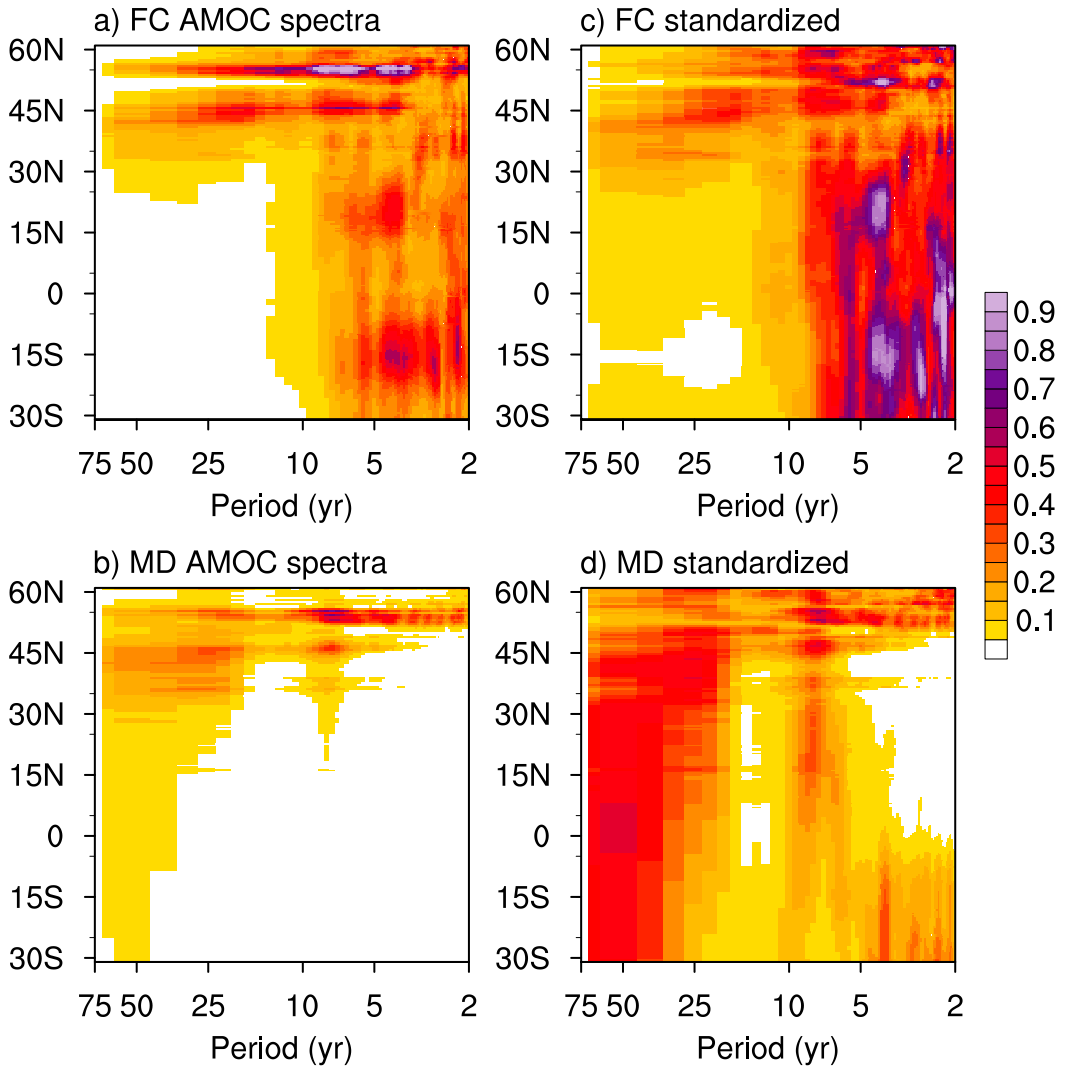

FIG. 4. Contour spectra showing spectral characteristics of the AMOC strength as a function of latitude. (a),(b) Contour spectra of the AMOC strength time series at every latitude in the (a) FC and (b) MD. Units are Sv^2 cpy. (c),(d) As in (a),(b), but each AMOC strength time series at each latitude is standardized before computing the spectrum. This allows one to visualize the dominant time scales contributing to the AMOC at each latitude, even if the amplitude of AMOC variability at that latitude is small. Units are standard deviation^2 cpy. To compute each spectrum, the time series is divided into four nonoverlapping 150-yr windows, the variance-preserving spectrum is computed over each window, and the average of the four spectra is plotted.

spectra help identify peaks that are generally common among the four 150-yr periods and help alleviate some of the noisiness seen in the full time series spectra.

The MD contour spectra (Fig. 4b) reveal that in the subpolar gyre, the buoyancy-driven AMOC exhibits variance across time scales, from interannual to multidecadal. In the subtropical gyre, little variance occurs on any time scale, but the variability that does occur is primarily at decadal or multidecadal time scales, as indicated by the standardized contour spectra (Fig. 4d). This suggests the potential presence of interhemispheric buoyancy-forced AMOC variability on low-frequency time scales. These results show that even though buoyancy drives AMOC variations in the subpolar gyre on interannual to multidecadal time scales, primarily low frequencies penetrate into the subtropical gyre (Johnson and Marshall 2002a,b, 2004; Böning et al. 2006; Zou et al. 2019).

In the FC, AMOC variability in the subtropics is dominated by high variance wind-driven variability (Figs. 4a,c). At 26°N, the MD shows less variance than the FC at time scales of 2–10 years (Figs. 5c,d), consistent with subtropical AMOC variability being primarily wind-driven as seen in the Ocn_{flux} experiments and

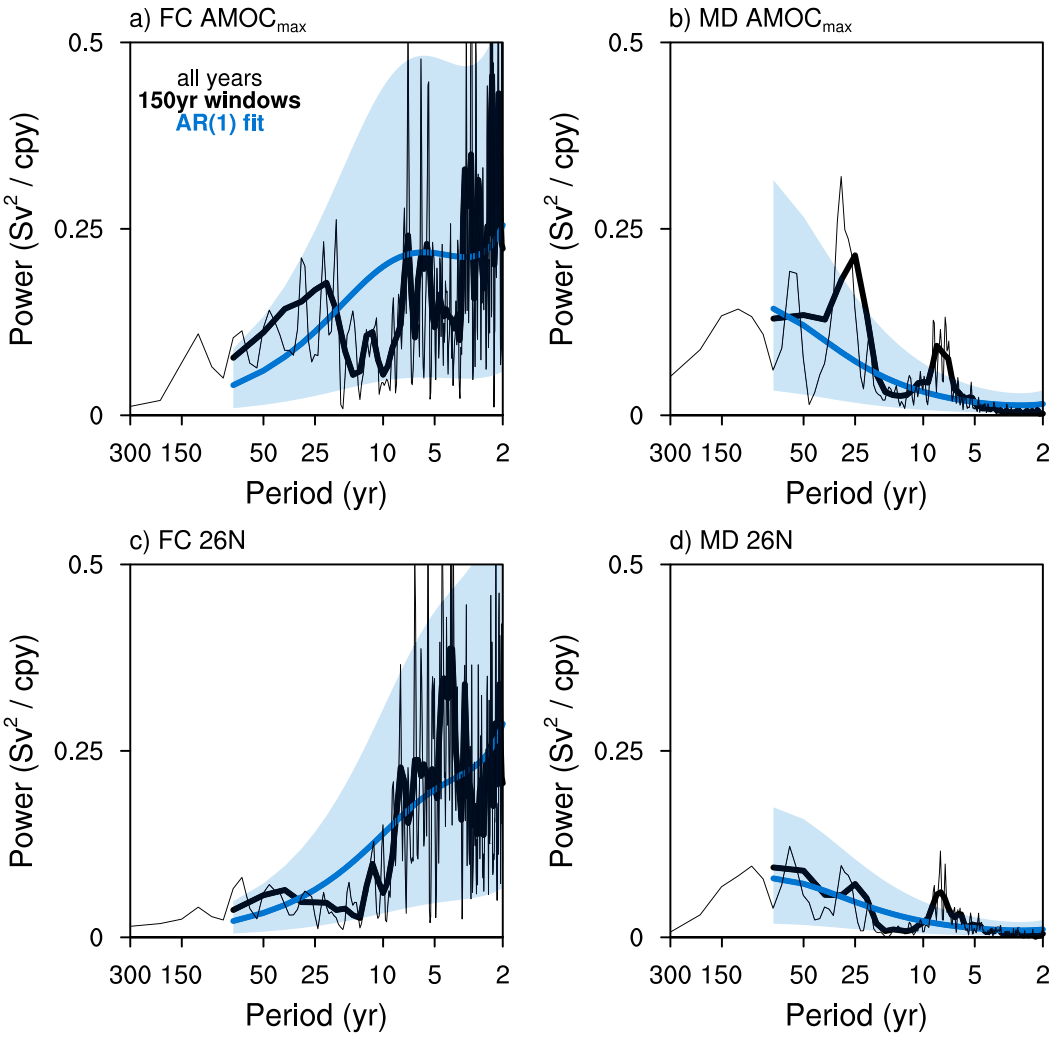

FIG. 5. Variance-preserving spectral analyses for (a) the FC AMOC$_{max}$ and (b) the MD AMOC$_{max}$ time series. The black thin line depicts the spectrum computed over the full 600-yr time series. The black bold curve depicts the average spectrum computed over four nonoverlapping 150-yr windows. The blue bold curve depicts the AR(1) fit for the window-averaged spectrum with the respective 95% confidence interval shaded. (c),(d) As in (a),(b), but for the AMOC strength time series computed at 26°N.

observed estimates (Zhao and Johns 2014). In the subpolar gyre, the FC AMOC exhibits variability on interannual to multidecadal time scales. The magnitude of the variance is larger than that in the MD (cf. Figs. 4a,b), indicating that AMOC variations in the subpolar gyre also have a wind-driven component. For the AMOC$_{max}$ (i.e., variability at ~45°N) the MD spectrum shows near-zero variance at periods shorter than 5 years (cf. Figs. 5a,b), indicating that buoyancy forcing does not contribute substantially to AMOC variations on these time scales. Both wind and buoyancy forcing contribute to variations in AMOC strength for time scales of 5–20 years; for time scales longer than 20 years, buoyancy forcing appears to dominate.

3) AMOC SPATIAL PATTERNS

Third, we consider the spatial patterns of AMOC variability by 1) looking at the spatial patterns of AMOC variability associated with AMOC$_{max}$ and 2) performing an empirical orthogonal function (EOF) analysis to extract the dominant modes of AMOC variability.

The spatial patterns of the AMOC associated with the AMOC$_{max}$ index are found by computing the correlation between the AMOC$_{max}$ time series and AMOC anomalies at each latitude and depth. For both the FC and MD, the correlations are near one at ~45°N, reflecting that AMOC$_{max}$ extracts variability near 45°N (Figs. 6a,b). In the MD, correlations are high throughout

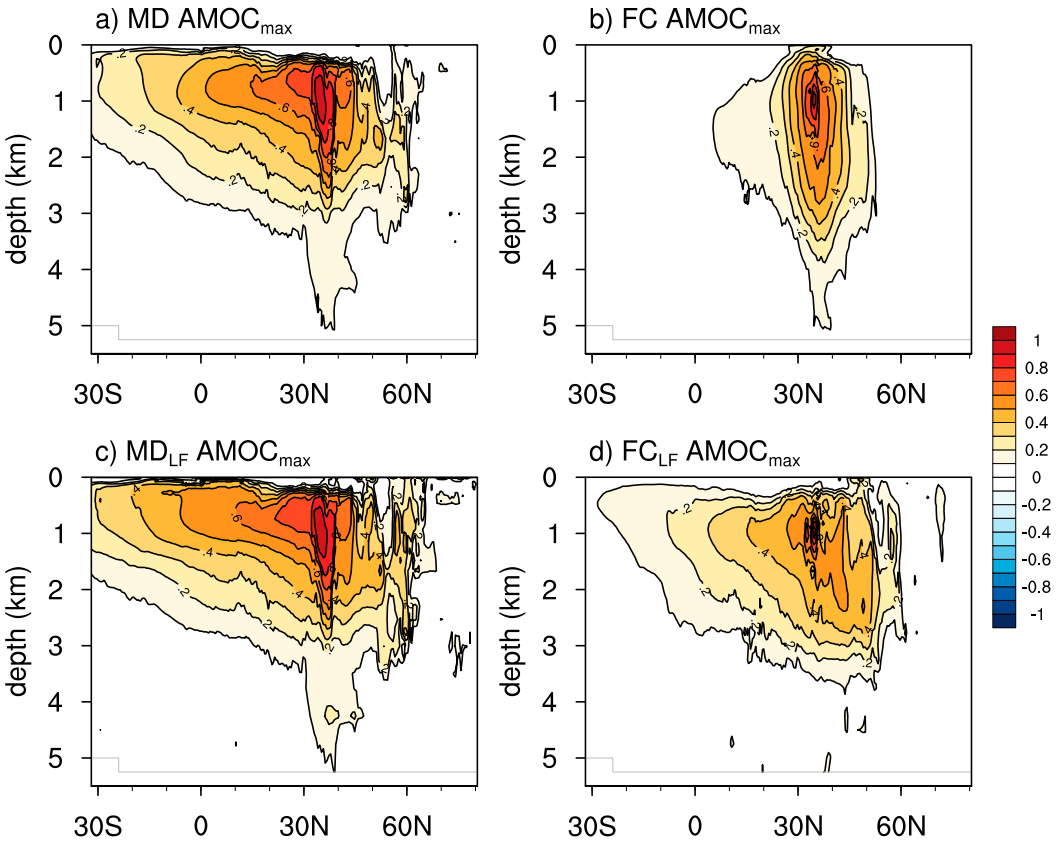

FIG. 6. Latitude vs depth profile of the correlation between the $AMOC_{max}$ time series and AMOC anomalies at each latitude and depth for (a) MD and (b) FC. (c),(d) As in (a),(b), but both the $AMOC_{max}$ index and the AMOC anomalies are low-frequency filtered (10-yr low-pass Lanczos filter) prior to computing the correlation.

the basin, demonstrating that the $AMOC_{max}$ index well represents interhemispheric AMOC variability. In the FC, however, high temporal covariability (correlations > 0.5) between the AMOC and $AMOC_{max}$ is meridionally confined near 30°–50°N. When considering only low frequencies (cutoff filter is 10 years), the FC_{LF} $AMOC_{max}$ extracts the interhemispheric pattern (Fig. 6d), but the correlations are smaller compared to the MD (Fig. 6c). Even at low frequencies, $AMOC_{max}$ does not represent purely buoyancy-driven AMOC variations at low latitudes due to the presence of wind-driven variability.

Next, we perform thickness-weighted EOF analyses over 30°–60°N to isolate the dominant spatial pattern of AMOC variability. In the MD, EOF1 (Fig. 7a) extracts a large-scale interhemispheric pattern with a maximum in the NH subpolar gyre, characteristic of the canonical AMOC pattern. The principal component time series (PC1; Fig. 7e) exhibits a broad peak in variance on multidecadal time scales and a secondary peak at interannual time scales (~8 yr; Fig. 7i). This indicates a large-scale pattern of buoyancy-driven AMOC variability on interannual and multidecadal time scales. Note that this pattern of variability is unrelated to El Niño–Southern Oscillation (ENSO), because, by definition, there is no active Bjerknes feedback in the MD and thus no canonical ENSO variability (Larson and Kirtman 2015). In the FC, EOF1 (Fig. 7b) extracts an interhemispheric pattern symmetric about the equator but maximized within the subtropical latitudes. The PC1 time series (Fig. 7f) has the largest variance on interannual time scales (<8 yr; Fig. 7j), indicative of a significant wind-driven contribution.

We have seen differences between the FC and MD AMOC in terms of total variances (Fig. 3), temporal variability (Figs. 4 and 5), meridional covariability (Fig. 6), and dominant patterns of variability (Figs. 7a,b). However, after low-pass filtering the FC, the FC_{LF} EOF1 (Fig. 7d) extracts a similar pattern as the MD. This pattern explains 60% of the FC_{LF} AMOC variance, whereas the same pattern in the MD_{LF} (Fig. 7c) explains 73% of the variance, suggesting that even at low frequencies, wind variability contributes to the FC AMOC variance (Böning et al. 2006; Biastoch et al. 2008). The temporal statistics of the low-frequency PC1 are not the same, however (cf. Figs. 7g,h).

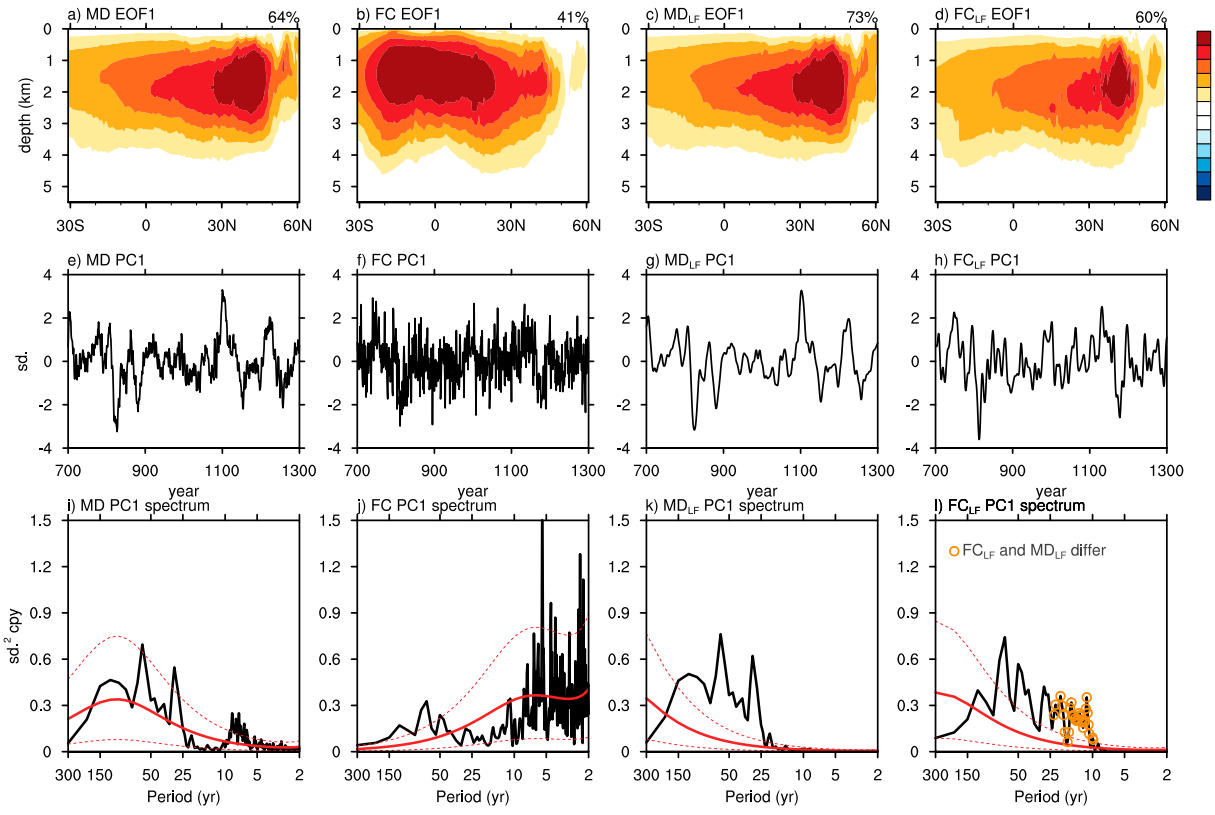

FIG. 7. An EOF analysis to determine the dominant spatial patterns of AMOC variability. (a)–(d) EOF1 pattern of the annual AMOC variability in the (a) MD and (b) FC, and (c),(d) the 10-yr low-pass filtered versions (MD_{LF} and FC_{LF}) in Sv per unit standard deviation of the respective principal component (PC1) time series, (e)–(h) the respective standardized PC1 time series, and (i)–(l) the variance-preserving spectrum of the standardized PC1 time series. Each solid red curve indicates the AR(1) fit and the red dashed curves depict the respective 95% confidence interval. In (l), orange circles indicate at what periods the variance of the FC_{LF} PC1 spectrum is significantly different from the variance of the MD_{LF} PC1 spectrum. Significance is determined using a Fisher's F test at the 99% confidence level. To estimate the effective degrees of freedom, N_{eff}, we divide the $N = 600$ samples by 2 × decorrelation time scale of the respective PC1 time series (17 yr for both the MD and MD_{LF}; 13 yr for the FC; 16 yr for the FC_{LF}). We estimate the decorrelation time scale by the number of years it takes for the lag-0 autocorrelation to drop below 0.1. The resulting N_{eff} values are 18 for the MD and MD_{LF}, 19 for the FC_{LF}, and 23 for the FC.

Consideration of the variance-preserving power spectra shows that PC1 for the FC_{LF} exhibits larger variability on time scales between 10 and 25 years when compared to the MD_{LF} PC1, as denoted by periods with orange circles in Fig. 7l (orange circles identify statistically significant differences between the MD_{LF} and FC_{LF} at the 99% confidence level). These time scales are just over the filter cutoff period, suggesting that higher variance in the FC_{LF} is likely a by-product of the filter operating over a noisy (presumably due to wind variability) dataset (Cane et al. 2017). Similarly, if the cutoff period is changed to 5 or even 20 years, erroneous peaks emerge at time scales just over the specified filter cutoff period (not shown). So, one can extract the dominant large-scale pattern of buoyancy-driven AMOC variability by low-pass filtering the FC, but the statistics of the temporal variability will not be the same.

b. *Meridional ocean heat transport variations*

As detailed in the introduction, the canonical pattern of AMOC variability is associated with large-scale variations in meridional heat transport. Here, we characterize the Atlantic Ocean heat transport (OHT) variations and determine the variations associated with the canonical AMOC pattern in both the FC and MD.

To place the OHT variations related to the AMOC in context, we first describe the main features of the meridional OHT variations in both the FC and MD. The OHT variance is much larger in the FC than the MD for all latitudes south of 45°N, indicating that OHT variations at these latitudes are primarily wind driven (Fig. 8a). Buoyancy-driven variability (i.e., the MD) accounts for less than 15% of the OHT variability averaged over the subtropics from 30°S to 30°N in the FC. North of 45°N, the OHT variance in MD is similar to FC, indicating that at

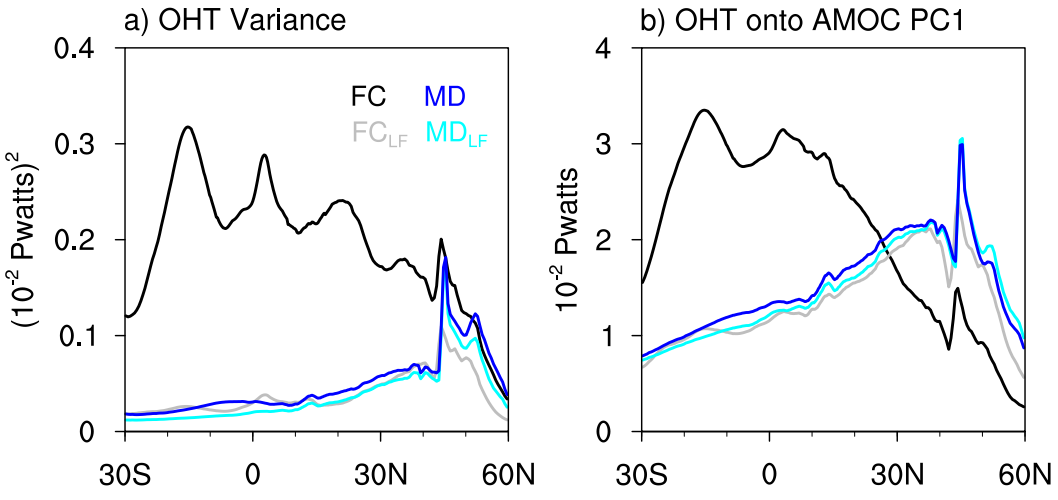

FIG. 8. (a) Total Atlantic Ocean heat transport (OHT) anomaly variance in the FC and MD simulations and the 10-yr low-pass filtered versions (MD_{LF} and FC_{LF}). Units are $(10^{-2}$ PW$)^2$. (b) OHT anomaly regressed onto the standardized PC1 time series of annual AMOC anomalies and low-frequency AMOC anomalies from the FC and MD. The PC1 time series are those in Figs. 7e–h. Units are 10^{-2} PW per unit standard deviation of the respective PC1 time series. The OHT anomalies are those due to Eulerian-mean advection over the Atlantic basin.

these latitudes OHT variations are primarily buoyancy forced. Between 45° and 60°N in the subpolar gyre, buoyancy-driven variability accounts for about 95% of the total OHT variance in the FC (low-frequency buoyancy-driven variability accounts for 75%). When low-pass filtered, the FC_{LF} OHT variance (Fig. 8a, gray curve) generally reproduces the MD profile, which demonstrates that most of the wind-driven OHT variations are at high frequencies. However, there are some subtleties in the subpolar gyre. 1) Low-pass filtering the MD reduces the OHT variance (cf. blue and cyan curves in Fig. 8a) because, like the AMOC (see Figs. 3b,e and 4b), buoyancy-forced Atlantic OHT exhibits high-frequency variations in the subpolar gyre. 2) Similar to the AMOC (see Fig. 3f), wind variability reduces the low-frequency variance of the OHT (cf. cyan and gray curves in Fig. 8a). This indicates that wind-driven variability reduces the detectability of low-frequency buoyancy-driven OHT in the subpolar gyre.

To determine the OHT variations that are associated with AMOC variations, we regress the OHT anomalies onto the PC1 time series of the AMOC (Fig. 8b). Recall that in the FC, the canonical AMOC pattern is recovered as EOF1 only when the AMOC is low-pass filtered (FC_{LF}) prior to computing the EOFs (Fig. 7d), whereas in the MD the canonical AMOC pattern is related to PC1 for both the unfiltered and low-pass filtered AMOC (Figs. 7a,c). It is clear that the canonical AMOC pattern is associated with northward OHT anomalies throughout the entire Atlantic basin in both the FC_{LF} (Fig. 8b, gray curve) and MD (Fig. 8b, blue and cyan curves). The OHT variations associated with the canonical AMOC include cross-equatorial OHT. The OHT variations are largest between 30° and 50°N and peak strongly at 45°N, where the maximal AMOC variations occur.

For the FC, recall that the unfiltered EOF1 of annual AMOC anomalies extracts an interhemispheric mode, but this pattern is quite different from the canonical AMOC pattern. The FC pattern appears largely wind-driven: it has maximum loading over the low latitudes (Fig. 7b) and variations are strongest at high frequencies (Figs. 7f,j). This pattern is associated with large OHT variations, including significant cross-equatorial OHT (Fig. 8b, black curve). Unlike the OHT variations associated with the canonical AMOC pattern, these OHT variations peak in the tropics and decline poleward of 15° in both hemispheres. The OHT anomalies associated with the FC PC1 are significantly stronger than those associated with the canonical AMOC pattern. However, these OHT variations may be less effective in driving a climate response as they otherwise would be in the midlatitudes due to the fact that in the tropics/subtropics, OHT variations related to wind-driven Ekman transports tend to oppose SST anomalies created by air–sea heat fluxes (Larson et al. 2018).

c. *Connection to the horizontal circulation and Gulf Stream*

To estimate the relationship between the NH gyre circulations and the AMOC in the coupled model, we regress the annual barotropic streamfunction (BSF) anomalies onto the standardized FC_{LF} and MD_{LF} PC1

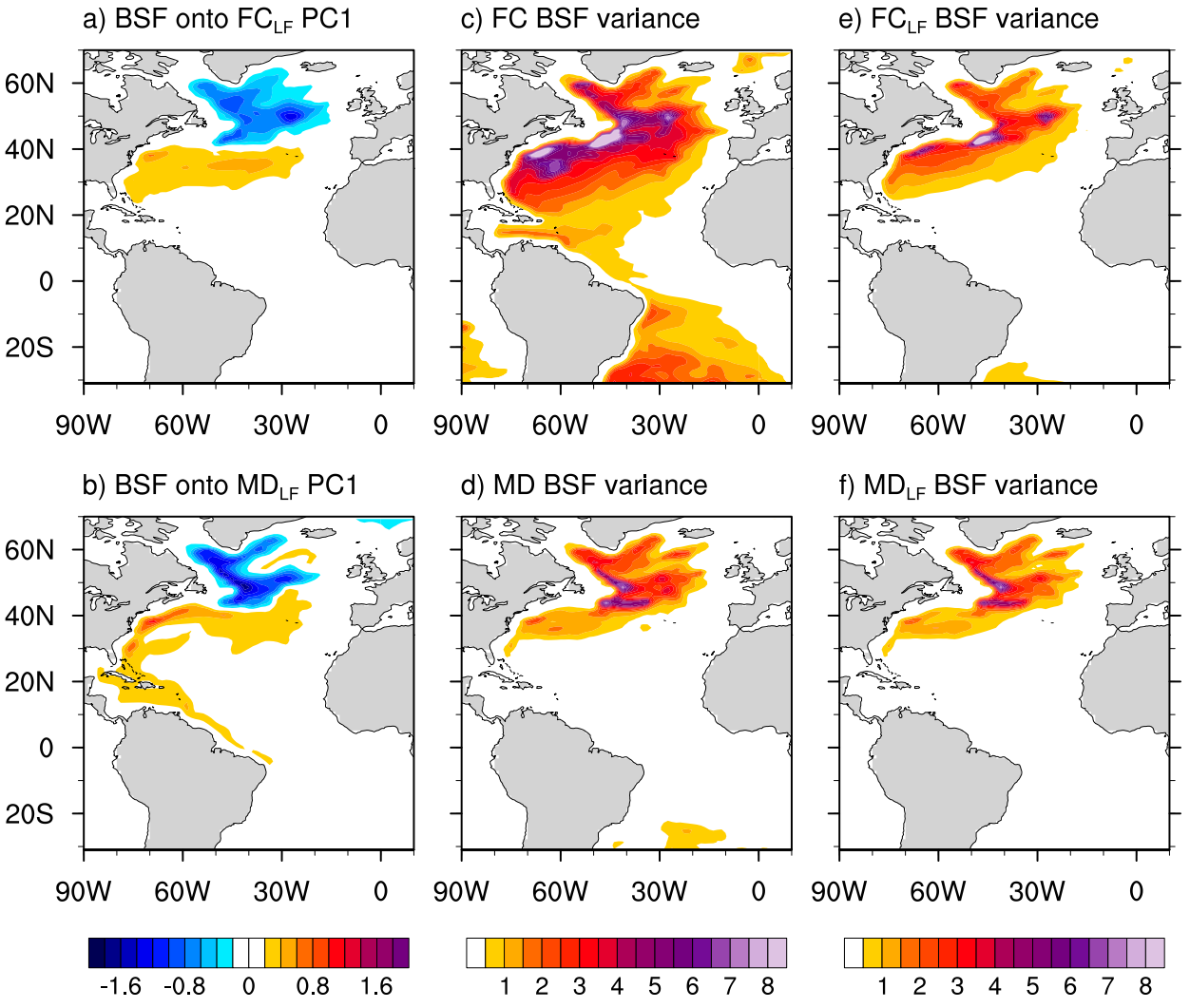

FIG. 9. (a),(b) Barotropic streamfunction (BSF) anomalies regressed onto the standardized PC1 time series associated with EOF1 of low-frequency AMOC anomalies from (a) the FC and (b) MD. Units are Sv per unit standard deviation of the respective PC1 time series. (c),(d) BSF anomaly variance from the FC and MD. (e),(f) As in (c),(d), but for the 10-yr low-pass filtered BSF anomaly variance. Units are Sv^2.

time series (unfiltered MD PC1 yields similar results), which are associated with the same canonical AMOC pattern in both simulations. In the MD, a stronger (weaker) buoyancy-driven AMOC is associated with an intensification (weakening) of the subpolar gyre (Fig. 9b). A stronger AMOC is also associated with intensification of the subtropical gyre, the GS, and the North Brazil Current. Low-pass filtering the FC AMOC (FC$_{LF}$; Fig. 9a) extracts a similar strengthening of the gyre circulations but does not depict nearly as strong of an intensification of the GS or the North Brazil Current. This suggests that wind variability overwhelms buoyancy-driven GS fluctuations in the FC model, even when only considering low frequencies.

Would AMOC-related changes in the NH gyre circulations be detectable in the presence of wind-driven variability? Comparing the BSF anomaly variance maps from the FC and MD (Figs. 9c,d) demonstrates that buoyancy forcing accounts for only a small fraction of the total BSF variance in the subtropical gyre and the GS region in the FC. This remains true when only considering low frequencies (Figs. 9e,f). This suggests that attempts to detect buoyancy-driven AMOC-related changes in the subtropical gyre circulation may be stymied by the abundance of wind-driven variability across time scales. In contrast, in the subpolar gyre, buoyancy forcing accounts for a significant portion of the circulation variability in the FC (Figs. 9c,d), and the buoyancy contribution is primarily at low frequencies (Fig. 9f), as argued in Yeager (2015). This further suggests that the subpolar gyre may be more promising to detect buoyancy-driven AMOC-related variability, as argued in Böning et al. (2006). Sustained observations of the ocean circulation in the subpolar

gyre are now being collected as part of the OSNAP program (Lozier et al. 2017).

Our results are consistent with the same-sign relationship between the strength of the AMOC and subpolar gyre found in Böning et al. (2006) and Yeager (2015) and opposite to that found in Zhang (2008). In the subtropical gyre, results appear consistent with de Coëtlogon et al. (2006), who connect a stronger AMOC to a stronger GS in ocean-only models. Prior studies have also connected shifts in the path of the GS to variations in AMOC strength (de Coëtlogon et al. 2006; Joyce and Zhang 2010); we choose to not emphasize potential GS path changes in CCSM4, given that the GS is poorly resolved (Siqueira and Kirtman 2016). Our results also demonstrate that variations in the GS in CCSM4 are dominated by wind-driven processes, even at low frequencies (cf. Figs. 9e,f). All of these results suggest that the relationship between AMOC variability and variations in the horizontal gyre circulations and GS seen in CCSM4 are likely related to surface processes (e.g., such as the common driving of the AMOC, the BSF, and the GS by the North Atlantic Oscillation) rather than deep ocean processes (e.g., changes in the Deep Western Boundary Current). The time series of North Brazil Current transport variations has also been linked to and proposed as a proxy for AMOC variations (Zhang et al. 2011), although Rühs et al. (2015) questioned its usefulness given the abundance of local wind-driven effects. Consistent with this idea, the North Brazil Current signal associated with the buoyancy-driven AMOC appears to be difficult to extract even when excluding high frequencies (Fig. 9a).

4. Summary

The goal of this study is to determine whether the characteristics typically ascribed to the buoyancy-driven AMOC (see the introduction) emerge in a coupled model that is only buoyancy forced. To do so, we compare a fully coupled (FC) version of CCSM4 with a mechanically decoupled (MD) version. In the MD, anomalous wind stress does not drive changes in the ocean circulation but wind variations are applied in the calculations of air–sea buoyancy fluxes via bulk formulas. It follows that in the MD, oceanic variability, including the AMOC, is by definition buoyancy forced, whereas oceanic variations in the FC are both buoyancy and wind forced.

The canonical AMOC is thought to be primarily buoyancy forced and characterized by several key attributes. To summarize, we list each attribute of the canonical AMOC, report whether the MD reproduces these attributes, and determine whether each can be extracted in the FC by low-pass filtering the AMOC, a common method used to isolate the buoyancy-driven AMOC pattern. In other words, we test whether the assumption that there is a time scale separation between high-frequency, wind-forced AMOC variations and low-frequency, buoyancy-forced AMOC variations is valid in our model. We also examine the relative magnitude of the canonical AMOC variations compared to the total AMOC variations, in order to determine whether buoyancy-driven AMOC variations are detectable in the presence of wind-driven variability.

- A low-frequency time scale: The buoyancy-driven AMOC in the MD is predominantly at low frequencies, but in the subpolar gyre, buoyancy-forced AMOC variations occur on time scales from interannual to multidecadal (Fig. 4). Low-pass filtering the FC does not reproduce the statistics of the temporal variability of the buoyancy-driven AMOC in its entirety (e.g., zero variance in 2–10-yr frequency bands; too high of variance at periods just higher than the 10-yr cutoff filter; see Fig. 7l). Even when low-pass filtered, the presence of wind-driven variability in the FC results in roughly a 50% reduction in low-frequency AMOC variance between 1- and 3-km depth compared to the purely buoyancy-driven AMOC in the MD (Fig. 3).
- Single cell meridional overturning circulation with maximum in the NH subpolar gyre: An EOF analysis shows that buoyancy-driven AMOC variability in the MD is characterized by the canonical AMOC structure (Fig. 7a). One can reproduce this dominant large-scale pattern of the buoyancy-driven AMOC by low-pass filtering the FC AMOC before computing the EOF (Fig. 7d), yet the spectral characteristics differ at both interannual and decadal time scales (Figs. 7i,l). Wind forcing substantially reduces the meridional coherence of the AMOC, even when the AMOC is low-pass filtered (Fig. 6).
- Connection to variations in Atlantic Ocean heat transport: A stronger canonical AMOC in the MD is associated with enhanced northward oceanic heat transport from 30°S to 60°N in the Atlantic, peaking at about 45°N (Fig. 8b). However, the FC model also exhibits significant wind-driven cross-equatorial AMOC and OHT anomalies (Fig. 8). Low-pass filtering the FC generally reproduces the latitudinal profile of OHT associated with the canonical AMOC pattern in the MD but with a slight reduction of AMOC-related OHT in both the low and high latitudes. Detecting ocean heat transport variations associated with the canonical AMOC pattern in the subtropical gyre is questionable because buoyancy accounts for less than 15% of the OHT variability there in the FC; the subpolar gyre is

more promising, as buoyancy accounts for 95% of the OHT variability.

- Connection to the strength of the NH gyre circulations and the Gulf Stream: In the MD, a stronger buoyancy-driven AMOC is associated with stronger NH gyre circulations and intensification of the GS and North Brazil Current (Fig. 9b). Buoyancy forcing accounts for only a small fraction of the variability in the subtropical gyre circulation in the FC model (Figs. 9c,d), suggesting that in the real world AMOC-related subtropical gyre variations are likely to be swamped by wind-driven variations. Low-pass filtering the AMOC in the FC reproduces the fluctuations in the strength of the NH gyre circulations seen in MD but not the strength of the AMOC–GS connection. This suggests that wind variability, even when only considering low frequencies, overwhelms buoyancy-driven GS variations. However, variations in the subpolar gyre circulation are primarily at low frequencies and buoyancy forced (Figs. 9c–f), further supporting the argument that detection of buoyancy-driven circulation anomalies in the subpolar gyre are promising.

Overall, these results clearly demonstrate that low-frequency filtering the AMOC can reproduce the buoyancy-driven AMOC pattern and associated attributes, with the exception of the North Brazil Current and GS signals, but the statistics of the temporal variability will differ. This means that when low-pass filtering the AMOC, one can easily misinterpret variability of these patterns as being solely linked to the buoyancy forcing. In reality, low-frequency wind-driven variability may still be present (Böning et al. 2006; Biastoch et al. 2008; Polo et al. 2014; Yeager and Danabasoglu 2014), high-frequency buoyancy-driven variability (Bingham et al. 2007) is excluded, the low-pass filter itself may generate erroneous peaks at time scales just longer than the cutoff filter (Cane et al. 2017), and wind variability can disrupt the penetration of buoyancy-forced signals into the subtropical gyre or swamp the buoyancy-forced signal altogether (Böning et al. 2006; Baehr et al. 2008; Rühs et al. 2015).

Similarities in our coupled model results and those found via forced, ocean, and sea ice–only hindcast CESM1 experiments with the same ocean model used in our coupled setup (Yeager and Danabasoglu 2014; Yeager 2015) are encouraging and suggest that conclusions based on the these previous studies can generally be extended to coupled versions of the model. Similar to our conclusions, Yeager and Danabasoglu (2014) find that buoyancy primarily drives meridionally coherent decadal AMOC variations and that wind variability introduces meridional asymmetry. Both previous studies find that the subpolar gyre in POP2, the same ocean model as in the MD and FC simulations, is primarily buoyancy driven. With the MD experiment, we find that the coupled model exhibits similar behavior as the forced ocean-only experiments and that the buoyancy-driven subpolar variations are mostly on decadal and multidecadal time scales (Fig. 9f).

5. Discussion

Comparison of the FC and MD AMOC accentuates the fact that the subpolar and subtropical gyres are very different places and this has implications for how one chooses to estimate AMOC variations in models and measure AMOC characteristics in the real ocean. In the subpolar gyre, the AMOC has significant low-frequency variability, buoyancy forcing is important on time scales from interannual to multidecadal (Figs. 4b,d), and the gyre circulation is primarily low-frequency and buoyancy forced (Figs. 9c–f). Subpolar variations in meridional heat transport are also primarily buoyancy-driven and low-frequency (Fig. 8a). In the subtropical gyre, AMOC variations are primarily wind forced on high frequencies (Figs. 4 and 5c,d) and the gyre circulation and Gulf Stream variations are mostly high-frequency and wind-forced (Figs. 9c–f). Variability in low-latitude meridional heat transport is primarily wind-forced and high-frequency (Fig. 8a).

Since buoyancy-driven AMOC variations and the AMOC-GS connection are obscured by high variance wind-driven variations in the low latitudes, subtropical gyre characteristics are not a good proxy for the canonical AMOC. Even low-pass filtering the subtropical AMOC does not accentuate the buoyancy-driven contribution and instead maximal variance tends to occur on time scales just longer than the cutoff frequency of the filter. Subpolar AMOC variations appear to be a better representation of the buoyancy-driven AMOC pattern, but estimating buoyancy-driven AMOC variations from subpolar AMOC variations comes with many caveats. In the real ocean and coupled models, wind variability reduces the meridional coherence of the AMOC, even when only considering low frequencies. Therefore, low-pass filtering the AMOC may not fully reproduce buoyancy-forced AMOC variations. Additionally, the buoyancy-forced AMOC has interhemispheric variations on interannual time scales (Fig. 7i), and low-pass filtering will remove these signals.

Our results have implications for typically used AMOC indices, such as $AMOC_{max}$ (e.g., Delworth et al. 1993; Msadek et al. 2010; Danabasoglu et al. 2012b; Kwon and Frankignoul 2012; Yeager and Danabasoglu 2012; Delworth and Zeng 2016). In the presence of wind variability,

$AMOC_{max}$ is a poor proxy for AMOC variations in the subtropical gyre or GS region, as AMOC variations are only correlated with $AMOC_{max}$ in a narrow band of latitudes around 45°N (Fig. 6). This lack of meridional coherence in AMOC variability has been established through ocean-only surface flux forcing experiments (Biastoch et al. 2008), analysis of interannual meridional transport in various models (Bingham et al. 2007), and the review of Lozier (2010). Our results show that low-pass filtering $AMOC_{max}$ recovers some of the meridionally coherent buoyancy-driven AMOC signals, but correlations in the subtropical gyre are still significantly smaller than they would be in the absence of wind-driven variability. The low-frequency filtered $AMOC_{max}$ also, by definition, excludes high-frequency buoyancy-driven variability that appears nontrivial in our model. The nonhomogeneity of AMOC variations has prompted other investigators to question the validity of single AMOC indexes defined by the meridional overturning streamfunction (Vellinga and Wu 2004; Yeager and Danabasoglu 2012) or flow transports (Bingham et al. 2007; Rühs et al. 2015).

Our results also have implications for the commonly used approach of low-pass filtering the AMOC to extract buoyancy-driven AMOC variations. The approach of low-pass filtering to estimate the buoyancy-driven AMOC component assumes a time scale separation between the wind-driven and buoyancy-driven AMOC. We do not find evidence for such a separation in either the subtropical or subpolar gyre. In the subtropical gyre, the AMOC is mostly wind-forced and wind-forced variations obscure the buoyancy-forced signal even at low frequencies. In the subpolar gyre, the AMOC is primarily buoyancy forced and buoyancy forcing leads to variability across time scales. Therefore, if one hopes to account for all meridionally coherent, interhemispheric, buoyancy-driven AMOC variations and the associated impacts and/or attributes, ignoring interannual time scales will result in an incomplete picture.

The relative importance of wind and buoyancy forcing at various latitudes likely is model dependent. Viewing the contour spectra of AMOC variability for multiple models, following the analyses shown in Fig. 4a, would be an insightful first step in understanding the variety of AMOC temporal behavior in climate models. Although low-pass filtering the AMOC in CCSM4 is able to reproduce the spatial pattern of the canonical AMOC, this does not mean that this same filter can be applied to other models to extract the buoyancy-forced AMOC. For a true characterization of buoyancy-forced AMOC variations in other models, a similar MD approach is instructive. Another recent approach using an adjoint model to separate AMOC forcings also appears promising (Heimbach et al. 2011; Pillar et al. 2016; Smith and Heimbach 2019; Kostov et al. 2019). Without such techniques, one is likely to misinterpret low-pass filtered AMOC variability as recovering the full interhemispheric, buoyancy-driven AMOC characteristics.

Acknowledgments. The fully coupled CCSM4 data in this study is accessed from the NCAR Earth System Grid (ESG) online repository at https://www.earthsystemgrid.org/. SL thanks Ben Kirtman and Dan Vimont for discussions early on in this work. We also thank three anonymous reviewers for insightful comments that helped improve the manuscript. AC was supported by the NSF Climate and Large-Scale Dynamics program. MB was funded by the NOAA ESS Program (NA16OAR4310167), NASA Physical Oceanography Program (NNX17AH49G), and NSF (1558821).

APPENDIX

Implementation of the Mechanically Decoupled Framework

The inception of the mechanically decoupled configuration for CCSM4 is described in Larson and Kirtman (2015) and updated for the Community Earth System Model (CESM) code modifications in Larson et al. (2017). Mechanically decoupling within the model code is relatively simple and should be reproducible using other models provided that the model's wind stress climatology is readily available. When atmospheric model-derived wind stresses are passed from the coupler to ocean model (which occurs once per model day), the modified code manually overwrites the values with CCSM4/CESM climatological wind stress values. This way, although the atmospheric model freely generates atmospheric circulation variability that goes into the turbulent heat flux calculations, the ocean surface is only mechanically forced by climatological wind stress. There are no explicit changes in the model code buoyancy flux calculations; therefore, the MD remains buoyancy coupled similar to the FC. This means that the coupled model MD framework allows for consistent surface fluxes and the possibility of thermally coupled modes. When looking at monthly and longer time scale climate variations, prescribing monthly mean wind stress climatology, as opposed to daily climatology, appears to be sufficient at reproducing the approximate FC seasonal cycle [see Larson et al. (2017) for more details].

The version of the MD in this work is essentially CCSM4 integrated through the updated CESM architecture. The reader is referred to Larson et al. (2018) for additional description and SST diagnostics of the MD

configuration. The prescribed wind stress climatology in the MD is taken from the last 100 years of the 680-yr FC simulation integrated at the University of Miami; this FC simulation is also CCSM4 integrated through the CESM architecture. The 680-yr FC simulation is not analyzed in the present study.

REFERENCES

Baehr, J., K. Keller, and J. Marotzke, 2008: Detecting potential changes in the meridional overturning circulation at 26°N in the Atlantic. *Climatic Change*, **91**, 11–27, https://doi.org/10.1007/s10584-006-9153-z.

Biastoch, A., C. W. Böning, J. Getzlaff, J.-M. Molines, and G. Madec, 2008: Causes of interannual–decadal variability in the meridional overturning circulation of the midlatitude North Atlantic Ocean. *J. Climate*, **21**, 6599–6615, https://doi.org/10.1175/2008JCLI2404.1.

Bingham, R. J., C. W. Hughes, V. Roussenov, and R. G. Williams, 2007: Meridional coherence of the North Atlantic meridional overturning circulation. *Geophys. Res. Lett.*, **34**, L23606, https://aorg/10.1029/2007GL031731.

Böning, C. W., M. Scheinert, J. Dengg, A. Biastoch, and A. Funk, 2006: Decadal variability of subpolar gyre transport and its reverberation in the North Atlantic overturning. *Geophys. Res. Lett.*, **33**, L21S01, https://doi.org/10.1029/2006GL026906.

Buckley, M. W., and J. Marshall, 2016: Observations, inferences, and mechanisms of the Atlantic meridional overturning circulation: A review. *Rev. Geophys.*, **54**, 5–63, https://doi.org/10.1002/2015RG000493.

——, D. Ferreira, J.-M. Campin, J. Marshall, and R. Tulloch, 2012: On the relationship between decadal buoyancy anomalies and variability of the Atlantic meridional overturning circulation. *J. Climate*, **25**, 8009–8030, https://doi.org/10.1175/JCLI-D-11-00505.1.

Cane, M. A., A. C. Clement, L. N. Murphy, and K. Bellomo, 2017: Low-pass filtering, heat flux, and Atlantic multidecadal variability. *J. Climate*, **30**, 7529–7553, https://doi.org/10.1175/JCLI-D-16-0810.1.

Cheng, W., J. C. H. Chiang, and D. Zhang, 2013: Atlantic meridional overturning circulation (AMOC) in CMIP5 models: RCP and historical simulations. *J. Climate*, **26**, 7187–7197, https://doi.org/10.1175/JCLI-D-12-00496.1.

Cunningham, S. A., and Coauthors, 2007: Temporal variability of the Atlantic meridional overturning circulation at 26.5°N. *Science*, **317**, 935–938, https://doi.org/10.1126/science.1141304.

Danabasoglu, G., S. C. Bates, B. P. Briegleb, S. R. Jayne, M. Jochum, W. G. Large, S. Peacock, and S. G. Yeager, 2012a: The CCSM4 ocean component. *J. Climate*, **25**, 1361–1389, https://doi.org/10.1175/JCLI-D-11-00091.1.

——, S. G. Yeager, Y.-O. Kwon, J. J. Tribbia, A. S. Phillips, and J. W. Hurrell, 2012b: Variability of the Atlantic meridional overturning circulation in CCSM4. *J. Climate*, **25**, 5153–5172, https://doi.org/10.1175/JCLI-D-11-00463.1.

de Coëtlogon, G., C. Frankignoul, M. Bentsen, C. Delon, H. Haak, S. Masina, and A. Pardaens, 2006: Gulf Stream variability in five oceanic general circulation models. *J. Phys. Oceanogr.*, **36**, 2119–2135, https://doi.org/10.1175/JPO2963.1.

Delworth, T. L., and R. J. Greatbatch, 2000: Multidecadal thermohaline circulation variability driven by atmospheric surface flux forcing. *J. Climate*, **13**, 1481–1495, https://doi.org/10.1175/1520-0442(2000)013<1481:MTCVDB>2.0.CO;2.

——, and F. Zeng, 2012: Multicentennial variability of the Atlantic meridional overturning circulation and its climatic influence in a 4000 year simulation of the GFDL CM2.1 climate model. *Geophys. Res. Lett.*, **39**, L13702, https://doi.org/10.1029/2012GL052107.

——, and ——, 2016: The impact of the North Atlantic Oscillation on climate through its influence on the Atlantic meridional overturning circulation. *J. Climate*, **29**, 941–962, https://doi.org/10.1175/JCLI-D-15-0396.1.

——, S. Manabe, and R. J. Stouffer, 1993: Interdecadal variations of the thermohaline circulation in a coupled ocean–atmosphere model. *J. Climate*, **6**, 1993–2011, https://doi.org/10.1175/1520-0442(1993)006<1993:IVOTTC>2.0.CO;2.

Dong, B.-W., and R. T. Sutton, 2002: Adjustment of the coupled ocean–atmosphere system to a sudden change in the thermohaline circulation. *Geophys. Res. Lett.*, **29**, 1728, https://doi.org/10.1029/2002GL015229.

Dunstone, N. J., and D. M. Smith, 2010: Impact of atmosphere and sub-surface ocean data on decadal climate prediction. *Geophys. Res. Lett.*, **37**, L02709, https://doi.org/10.1029/2009GL041609.

Eden, C., and J. Willebrand, 2001: Mechanism of interannual to decadal variability of the North Atlantic circulation. *J. Climate*, **14**, 2266–2280, https://doi.org/10.1175/1520-0442(2001)014<2266:MOITDV>2.0.CO;2.

Feulner, G., S. Rahmstorf, A. Levermann, and S. Volkwardt, 2013: On the origin of the surface air temperature difference between the hemispheres in Earth's present-day climate. *J. Climate*, **26**, 7136–7150, https://doi.org/10.1175/JCLI-D-12-00636.1.

Frierson, D. M. W., and Coauthors, 2013: Contribution of ocean overturning circulation to tropical rainfall peak in the Northern Hemisphere. *Nat. Geosci.*, **6**, 940–944, https://doi.org/10.1038/ngeo1987.

Gent, P. R., and Coauthors, 2011: The Community Climate System Model version 4. *J. Climate*, **24**, 4973–4991, https://doi.org/10.1175/2011JCLI4083.1.

Heimbach, P., C. Wunsch, R. M. Ponte, G. Forget, C. Hill, and J. Utke, 2011: Timescales and regions of the sensitivity of Atlantic meridional volume and heat transport: Toward observing system design. *Deep-Sea Res. II*, **58**, 1858–1879, https://doi.org/10.1016/j.dsr2.2010.10.065.

Hunke, E. C., and W. H. Lipscomb, 2008: CICE: The Los Alamos sea ice model user's manual version 4. Los Alamos National Laboratory Tech. Rep. LA-CC-06-012, 76 pp.

Johns, W. E., and Coauthors, 2011: Continuous, array-based estimates of Atlantic ocean heat transport at 26.5°N. *J. Climate*, **24**, 2429–2449, https://doi.org/10.1175/2010JCLI3997.1.

Johnson, H. L., and D. P. Marshall, 2002a: A theory for the surface Atlantic response to thermohaline variability. *J. Phys. Oceanogr.*, **32**, 1121–1132, https://doi.org/10.1175/1520-0485(2002)032<1121:ATFTSA>2.0.CO;2.

——, and ——, 2002b: Localization of abrupt change in the North Atlantic thermohaline circulation. *Geophys. Res. Lett.*, **29**, 1083, https://doi.org/10.1029/2001GL014140.

——, and ——, 2004: Global teleconnections of meridional overturning circulation anomalies. *J. Phys. Oceanogr.*, **34**, 1702–1722, https://doi.org/10.1175/1520-0485(2004)034<1702:GTOMOC>2.0.CO;2.

Joyce, T. M., and R. Zhang, 2010: On the path of the Gulf Stream and the Atlantic meridional overturning circulation. *J. Climate*, **23**, 3146–3154, https://doi.org/10.1175/2010JCLI3310.1.

Kang, S. M., I. M. Held, D. M. W. Frierson, and M. Zhao, 2008: The response of the ITCZ to extratropical thermal forcing:

Idealized slab-ocean experiments with a GCM. *J. Climate*, **21**, 3521–3532, https://doi.org/10.1175/2007JCLI2146.1.

——, D. M. W. Frierson, and I. M. Held, 2009: The tropical response to extratropical thermal forcing in an idealized GCM: The importance of radiative feedbacks and convective parameterization. *J. Atmos. Sci.*, **66**, 2812–2827, https://doi.org/10.1175/2009JAS2924.1.

Keenlyside, N. S., M. Latif, J. Jungclaus, L. Kornblueh, and E. Roeckner, 2008: Advancing decadal-scale climate prediction in the North Atlantic sector. *Nature*, **453**, 84–88, https://doi.org/10.1038/nature06921.

Kostov, Y., H. L. Johnson, and D. P. Marshall, 2019: AMOC sensitivity to surface buoyancy fluxes: The role of air–sea feedback mechanisms. *Climate Dyn.*, **53**, 4521–4537, https://doi.org/10.1007/s00382-019-04802-4.

Kuhlbrodt, T., A. Griesel, M. Montoya, A. Levermann, M. Hofmann, and S. Rahmstorf, 2007: On the driving processes of the Atlantic meridional overturning circulation. *Rev. Geophys.*, **45**, RG2001, https://doi.org/10.1029/2004RG000166.

Kwon, Y.-O., and C. Frankignoul, 2012: Stochastically-driven multidecadal variability of the Atlantic meridional overturning circulation in CCSM3. *Climate Dyn.*, **38**, 859–876, https://doi.org/10.1007/s00382-011-1040-2.

Larson, S. M., and B. P. Kirtman, 2015: Revisiting ENSO coupled instability theory and SST error growth in a fully coupled model. *J. Climate*, **28**, 4724–4742, https://doi.org/10.1175/JCLI-D-14-00731.1.

——, ——, and D. J. Vimont, 2017: A framework to decompose wind-driven biases in climate models applied to CCSM/CESM in the eastern Pacific. *J. Climate*, **30**, 8763–8782, https://doi.org/10.1175/JCLI-D-17-0099.1.

——, D. J. Vimont, A. C. Clement, and B. P. Kirtman, 2018: How momentum coupling affects SST variance and large-scale Pacific climate variability in CESM. *J. Climate*, **31**, 2927–2944, https://doi.org/10.1175/JCLI-D-17-0645.1.

Li, D., R. Zhang, and T. Knutson, 2018: Comparison of mechanisms for low-frequency variability of summer Arctic sea ice in three coupled models. *J. Climate*, **31**, 1205–1226, https://doi.org/10.1175/JCLI-D-16-0617.1.

Lozier, M. S., 2010: Deconstructing the conveyor belt. *Science*, **328**, 1507–1511, https://doi.org/10.1126/science.1189250.

——, 2012: Overturning in the North Atlantic. *Annu. Rev. Mar. Sci.*, **4**, 291–315, https://doi.org/10.1146/annurev-marine-120710-100740.

——, and Coauthors, 2017: Overturning in the subpolar North Atlantic program: A new international ocean observing system. *Bull. Amer. Meteor. Soc.*, **98**, 737–752, https://doi.org/10.1175/BAMS-D-16-0057.1.

Marshall, J., A. Donohoe, D. Ferreira, and D. McGee, 2014: The ocean's role in setting the mean position of the inter-tropical convergence zone. *Climate Dyn.*, **42**, 1967–1979, https://doi.org/10.1007/s00382-013-1767-z.

McCarthy, G. D., I. D. Haigh, J. J.-M. Hirschi, J. P. Grist, and D. A. Smeed, 2015: Ocean impact on decadal Atlantic climate variability revealed by sea-level observations. *Nature*, **521**, 508–510, https://doi.org/10.1038/nature14491.

Medhaug, I., H. R. Langehaug, T. Eldevik, T. Furevik, and M. Bentsen, 2012: Mechanisms for decadal scale variability in a simulated Atlantic meridional overturning circulation. *Climate Dyn.*, **39**, 77–93, https://doi.org/10.1007/s00382-011-1124-z.

Msadek, R., K. W. Dixon, T. L. Delworth, and W. Hurlin, 2010: Assessing the predictability of the Atlantic meridional overturning circulation and associated fingerprints. *Geophys. Res. Lett.*, **37**, L19608, https://doi.org/10.1029/2010GL044517.

Neale, R. B., J. Richter, S. Park, P. H. Lauritzen, S. J. Vavrus, P. J. Rasch, and M. Zhang, 2013: The mean climate of the Community Atmosphere Model (CAM4) in forced SST and fully coupled experiments. *J. Climate*, **26**, 5150–5168, https://doi.org/10.1175/JCLI-D-12-00236.1.

Oleson, K. W., and Coauthors, 2008: Improvements to the Community Land Model and their impact on the hydrological cycle. *J. Geophys. Res. Biogeosci.*, **113**, G01021, https://doi.org/10.1029/2007JG000563.

Pillar, H. R., P. Heimbach, H. L. Johnson, and D. P. Marshall, 2016: Dynamical attribution of recent variability in Atlantic overturning. *J. Climate*, **29**, 3339–3352, https://doi.org/10.1175/JCLI-D-15-0727.1.

Pohlmann, H., F. Sienz, and M. Latif, 2006: Influence of the multidecadal Atlantic meridional overturning circulation variability on European climate. *J. Climate*, **19**, 6062–6067, https://doi.org/10.1175/JCLI3941.1.

Polo, I., J. Robson, R. Sutton, and M. A. Balmaseda, 2014: The importance of wind and buoyancy forcing for the boundary density variations and the geostrophic component of the AMOC at 26°N. *J. Phys. Oceanogr.*, **44**, 2387–2408, https://doi.org/10.1175/JPO-D-13-0264.1.

Roberts, C. D., M. D. Palmer, R. P. Allan, D. G. Desbruyeres, P. Hyder, C. Liu, and D. Smith, 2017: Surface flux and ocean heat transport convergence contributions to seasonal and interannual variations of ocean heat content. *J. Geophys. Res. Oceans*, **122**, 726–744, https://doi.org/10.1002/2016JC012278.

Robson, J., R. Sutton, K. Lohmann, D. Smith, and M. D. Palmer, 2012: Causes of the rapid warming of the North Atlantic Ocean in the mid-1990s. *J. Climate*, **25**, 4116–4134, https://doi.org/10.1175/JCLI-D-11-00443.1.

Rühs, S., K. Getzlaff, J. V. Durgadoo, A. Biastoch, and C. W. Böning, 2015: On the suitability of North Brazil Current transport estimates for monitoring basin-scale AMOC changes. *Geophys. Res. Lett.*, **42**, 8072–8080, https://doi.org/10.1002/2015GL065695.

Sinha, B., B. Topliss, A. T. Blaker, and J.-M. Hirschi, 2013: A numerical model study of the effects of interannual time scale wave propagation on the predictability of the Atlantic meridional overturning circulation. *J. Geophys. Res. Oceans*, **118**, 131–146, https://doi.org/10.1029/2012JC008334.

Siqueira, L., and B. P. Kirtman, 2016: Atlantic near-term climate variability and the role of a resolved Gulf Stream. *Geophys. Res. Lett.*, **43**, 3964–3972, https://doi.org/10.1002/2016GL068694.

Smith, R., and Coauthors., 2010: The Parallel Ocean Program (POP) reference manual. Los Alamos National Laboratory Tech. Rep. LAUR-10-01853, 141 pp.

Smith, T., and P. Heimbach, 2019: Atmospheric origins of variability in the South Atlantic meridional overturning circulation. *J. Climate*, **32**, 1483–1500, https://doi.org/10.1175/JCLI-D-18-0311.1.

Srokosz, M. A., and H. L. Bryden, 2015: Observing the Atlantic meridional overturning circulation yields a decade of inevitable surprises. *Science*, **348**, 1255575, https://doi.org/10.1126/science.1255575.

Trenberth, K. E., and J. M. Caron, 2001: Estimates of meridional atmosphere and ocean heat transports. *J. Climate*, **14**, 3433–3443, https://doi.org/10.1175/1520-0442(2001)014<3433:EOMAAO>2.0.CO;2.

Vellinga, M., and P. Wu, 2004: Low-latitude freshwater influence on centennial variability of the Atlantic thermohaline circulation. *J. Climate*, **17**, 4498–4511, https://doi.org/10.1175/3219.1.

Xu, X., E. P. Chassignet, W. E. Johns, W. J. Schmitz, and E. J. Metzger, 2014: Intraseasonal to interannual variability of the Atlantic meridional overturning circulation from eddy-resolving simulations and observations. *J. Geophys. Res. Oceans*, **119**, 5140–5159, https://doi.org/10.1002/2014JC009994.

Yeager, S., 2015: Topographic coupling of the Atlantic overturning and gyre circulations. *J. Phys. Oceanogr.*, **45**, 1258–1284, https://doi.org/10.1175/JPO-D-14-0100.1.

——, and G. Danabasoglu, 2012: Sensitivity of Atlantic meridional overturning circulation variability to parameterized Nordic sea overflows in CCSM4. *J. Climate*, **25**, 2077–2103, https://doi.org/10.1175/JCLI-D-11-00149.1.

——, and ——, 2014: The origins of late-twentieth-century variations in the large-scale North Atlantic circulation. *J. Climate*, **27**, 3222–3247, https://doi.org/10.1175/JCLI-D-13-00125.1.

——, and J. I. Robson, 2017: Recent progress in understanding and predicting Atlantic decadal climate variability. *Curr. Climate Change Rep.*, **3**, 112–127, https://doi.org/10.1007/s40641-017-0064-z.

——, A. R. Karspeck, and G. Danabasoglu, 2015: Predicted slowdown in the rate of Atlantic sea ice loss. *Geophys. Res. Lett.*, **42**, 10 704–10 713, https://doi.org/10.1002/2015GL065364.

Zhang, D., M. J. McPhaden, and W. E. Johns, 2003: Observational evidence for flow between the subtropical and tropical Atlantic: The Atlantic subtropical cells. *J. Phys. Oceanogr.*, **33**, 1783–1797, https://doi.org/10.1175/2408.1.

——, R. Msadek, M. J. McPhaden, and T. Delworth, 2011: Multidecadal variability of the North Brazil Current and its connection to the Atlantic meridional overturning circulation. *J. Geophys. Res. Oceans*, **116**, C04012, https://doi.org/10.1029/2010JC006812.

Zhang, J., and R. Zhang, 2015: On the evolution of Atlantic meridional overturning circulation fingerprint and implications for decadal predictability in the North Atlantic. *Geophys. Res. Lett.*, **42**, 5419–5426, https://doi.org/10.1002/2015GL064596.

Zhang, R., 2008: Coherent surface–subsurface fingerprint of the Atlantic meridional overturning circulation. *Geophys. Res. Lett.*, **35**, L20705, https://doi.org/10.1029/2008GL035463.

——, and G. K. Vallis, 2007: The role of bottom vortex stretching on the path of the North Atlantic western boundary current and on the northern recirculation gyre. *J. Phys. Oceanogr.*, **37**, 2053–2080, https://doi.org/10.1175/JPO3102.1.

——, R. Sutton, G. Danabasoglu, Y.-O. Kwon, R. Marsh, S. G. Yeager, D. E. Amrhein, and C. M. Little, 2019: A review of the role of the Atlantic meridional overturning circulation in Atlantic multidecadal variability and associated climate impacts. *Rev. Geophys.*, **57**, 316–375, https://doi.org/10.1029/2019rg000644.

Zhao, J., and W. Johns, 2014: Wind-forced interannual variability of the Atlantic meridional overturning circulation at 26.5°N. *J. Geophys. Res. Oceans*, **119**, 2403–2419, https://doi.org/10.1002/2013JC009407.

Zou, S., M. S. Lozier, and M. Buckley, 2019: How is meridional coherence maintained in the lower limb of the Atlantic meridional overturning circulation? *Geophys. Res. Lett.*, **46**, 244–252, https://doi.org/10.1029/2018GL080958.